The selection function of the RAVE survey

Jennifer Wojno,[1][*] Georges Kordopatis,[1] Tilmann Piffl,[2] James Binney,[2] Matthias Steinmetz,[1] Gal Matijevič,[1] Joss Bland-Hawthorn,[3] Sanjib Sharma,[3] Paul McMillan,[4] Fred Watson,[5] Warren Reid,[6,7] Andrea Kunder,[1] Harry Enke,[1] Eva K. Grebel,[8] George Seabroke,[9] Rosemary F. G. Wyse,[10] Tomaž Zwitter,[11] Olivier Bienaymé,[12] Kenneth C. Freeman,[13] Brad K. Gibson,[14] Gerry Gilmore,[15] Amina Helmi,[16] Ulisse Munari,[17] Julio F. Navarro,[18] Quentin A. Parker,[19] Arnaud Siebert[12]

[1]*Leibniz Institut für Astrophysik Potsdam, An der Sternwarte 16, 14482 Potsdam, Germany*
[2]*Rudolf Peierls Centre for Theoretical Physics, 1 Keble Road, Oxford OX1 3NP, UK*
[3]*Sydney Institute for Astronomy, School of Physics A28, University of Sydney, NSW 2006, Australia*
[4]*Lund Observatory, Lund University, Department of Astronomy and Theoretical Physics, Box 43, SE-22100 Lund, Sweden*
[5]*Australian Astronomical Observatory, North Ryde, NSW 2113, Australia*
[6]*Department of Physics and Astronomy, Macquarie University, Sydney, NSW 2109, Australia*
[7]*Western Sydney University, Locked Bag 1797, Penrith South DC, NSW 1797, Australia*
[8]*Astronomisches Rechen-Institut, Zentrum für Astronomie der Universität Heidelberg, Mönchhofstr. 12–14, 69120 Heidelberg, Germany*
[9]*Mullard Space Science Laboratory, University College London, Holmbury St Mary, Dorking, RH5 6NT, UK*
[10]*Department of Physics and Astronomy, Johns Hopkins University, 3400 N. Charles St, Baltimore, MD 21218, USA*
[11]*Faculty of Mathematics and Physics, University of Ljubljana, 1000 Ljubljana, Slovenia*
[12]*Observatoire astronomique de Strasbourg, Université de Strasbourg, CNRS, UMR 7550, 11 rue de l'Université, F-67000 Strasbourg, France*
[13]*Research School of Astronomy & Astrophysics, Australian National University, Cotter Rd., Weston, ACT 2611, Australia*
[14]*E.A. Milne Centre for Astrophysics, University of Hull, Hull, HU6 7RX, United Kingdom*
[15]*Institute of Astronomy, Madingley Rd, Cambridge CB3 0HA, UK*
[16]*Kapteyn Astronomical Institute P.O. Box 800, 9700 AV Groningen, The Netherlands*
[17]*INAF Astronomical Observatory of Padova, I-36012 Asiago (VI), Italy*
[18]*Senior CIfAR Fellow. Department of Physics and Astronomy, University of Victoria, Victoria, BC V8P 5C2, Canada*
[19]*Department of Physics, Chong Yuet Ming Physics Building, The University of Hong Kong, Hong Kong*

ABSTRACT

We characterize the selection function of RAVE using 2MASS as our underlying population, which we assume represents all stars which could have potentially been observed. We evaluate the completeness fraction as a function of position, magnitude, and color in two ways: first, on a field- by-field basis, and second, in equal-size areas on the sky. Then, we consider the effect of the RAVE stellar parameter pipeline on the final resulting catalogue, which in principle limits the parameter space over which our selection function is valid. Our final selection function is the product of the completeness fraction and the selection function of the pipeline. We then test if the application of the selection function introduces biases in the derived parameters. To do this, we compare a parent mock catalogue generated using Galaxia with a mock-RAVE catalogue where the selection function of RAVE has been applied. We conclude that for stars brighter than I = 12, between 4000K < T_{eff} < 8000K and 0.5 < $\log g$ < 5.0, RAVE is kinematically and chemically unbiased with respect to expectations from Galaxia.

Key words: methods: data analysis – Galaxy: kinematics and dynamics – Galaxy: abundances – Galaxy: fundamental parameters

[*] E-mail: jwojno@aip.de (JW)

1 INTRODUCTION

In any statistical analysis it is fundamental to understand the relation between the objects for which data were obtained, and the underlying population from which the sample was drawn. This relation is called the selection function of the sample. Without this knowledge, it is difficult to accurately infer the general properties of a population.

Many large-scale astronomical surveys of Milky Way stars with data releases currently or soon available make some effort to characterize their selection function. The explicit quantification of the selection function of a stellar survey has been demonstrated by Schönrich & Binney (2009) for the Geneva-Copenhagen survey (GCS; Nordström et al. 2004), Bovy et al. (2012) for a sub-sample of the Sloan Extension for Galactic Understanding and Exploration survey (SEGUE; Yanny et al. 2009), Nidever et al. (2014) for the APO Galactic Evolution Experiment (APOGEE; Majewski et al. 2015), and Stonkutė et al. (2016) for the Gaia-ESO survey (Gilmore et al. 2012). A number of factors such as changes to the observing strategy, limitations due to instrumentation, or including different input catalogues can all affect the final resulting catalogue, so it is crucial to consider each of these aspects when characterising the selection function.

In this article we present a study of the selection function of the RAdial Velocity Experiment (RAVE) survey based on its most recent data release (DR5; Kunder et al. 2017), to facilitate the wider and more robust use of this publicly-available catalogue. This survey was among the first surveys in Galactic astronomy with the explicit purpose of producing a homogeneous and well-defined data set. To achieve this goal, the initial target selection was based purely on the apparent *I*-band magnitudes of the stars.

Based on the simplicity of the selection function a number of recent studies using RAVE data, reviewed in Kordopatis (2015), assumed the RAVE survey to be a kinematically unbiased sample to investigate models of our Galaxy. In particular, Sharma et al. (2014) briefly addressed the selection function with respect to ensuring their subsample was unbiased, by mimicking the target selection of RAVE directly using Monte Carlo realisations of their Galaxy models. However, here we aim to characterize the selection function of all stars available in DR5.

We present a short overview on the RAVE survey in Section 2, summarising the history of the survey with respect to the target selection and observing strategy. Our reduced sample for evaluating the selection function is described in Section 3. In Section 4 we present our results for two different ways of evaluating the selection function: field-by-field and by HEALPIX pixel. Then in Section 4.3 we incorporate the effects of the spectral analysis pipeline on the final catalogue. In Section 5, we present the method for generating our mock-RAVE catalogue, and compare it to a sample of RAVE DR5 stars. We then test for biases due to the selection function of RAVE, by comparing our mock-RAVE catalogue with a parent GALAXIA sample. Finally, we discuss the implications of these findings and our conclusions in Section 6.
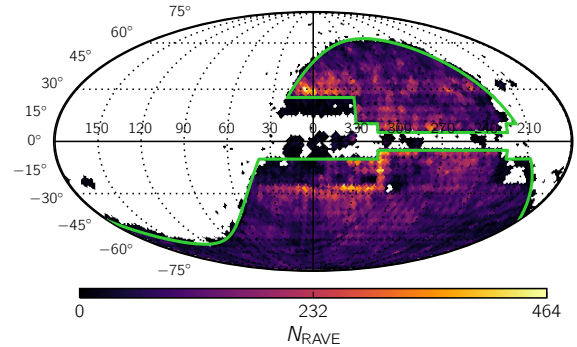

Figure 1. All RAVE DR5 targets in Galactic coordinates, colour-coded by number of stars in a given HEALPIX pixel (NSIDE = 32, area $\simeq 3.31 \deg^2$, see also Sec. 4.2). The adopted footprint (described in Sec. 2.3) is shown in green. In this study we only consider stars within the footprint.

2 THE RAVE SURVEY

RAVE is a large-scale spectroscopic stellar survey of the Southern hemisphere conducted using the 6dF multi-object spectrograph on the 1.2-m UK Schmidt Telescope at the Siding Spring Observatory in Australia, and completed in 2013. A general description of the project can be found in the data release papers (DR1; Steinmetz et al. 2006; DR2; Zwitter et al. 2008; DR3; Siebert et al. 2011; DR4; Kordopatis et al. 2013a) as well as in the most recent data release paper (DR5; Kunder et al. 2017). We show the distribution of targets available in RAVE DR5 in Figure 1.

The spectra were taken in the Ca II-triplet region (8410 – 8795 Å) with an effective spectral resolution of $R \approx 7500$. The strong calcium absorption lines allow a robust determination of the line-of- sight velocities via the Doppler effect even with low signal-to-noise ratio (SNR) ($\lesssim 10$ per pixel). This region was explicitly chosen to coincide with the spectral range of Gaia's Radial Velocity Spectrometer (RVS) (Prusti 2012; Bailer-Jones et al. 2013; Recio-Blanco et al. 2016). While Gaia will release radial velocity and stellar parameters in forthcoming data releases, at present Gaia offers only position and magnitude information for approximately a billion stars (Gaia Collaboration et al. 2016). The Tycho-Gaia astrometric solution (TGAS; Michalik et al. 2015) provides parallax and proper motion data for ~ 2 million stars which were observed by Tycho-2 (Høg et al. 2000). As RAVE contains 215 590 unique TGAS stars, it offers a unique advantage of providing stellar parameters for stars with improved parallax and proper motion data from TGAS.

2.1 Input catalogue

When observations for the RAVE survey started in 2003 there was no comprehensive photometric infrared survey available to serve as an input catalogue. Instead, approximate *I*-band magnitudes were calculated from the Tycho-2 catalogue and the SuperCOSMOS Sky Survey (SSS; Ham-
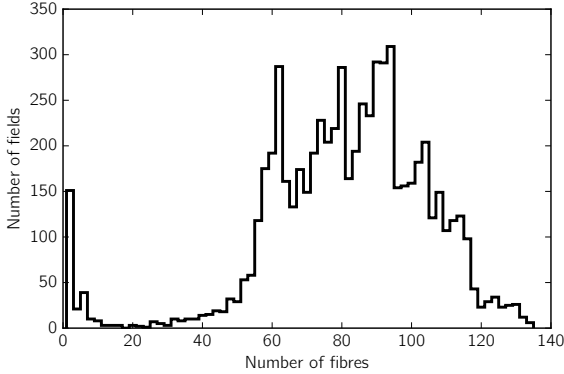
Figure 2. Histogram of the number of fibres placed for each pointing (bin width = 2), for the entire duration of the RAVE survey (2003-2013). For each pointing, at least one fibre was placed.

Figure 3. Distribution of I-magnitudes in the full RAVE DR5 catalogue. Dotted lines mark the border of the magnitude bins used for observing runs after March 2006. The histogram shows I_{2MASS} magnitudes which are computed from the 2MASS J and K_s magnitudes, but present a homogeneous database.

bly et al. 2001), and used to construct an initial input catalogue of ~300 000 stars. In May 2005, the DENIS catalogue (Epchtein et al. 1999) became available which provided Gunn I-band photometry, however, it did not provide sufficient sky coverage to serve as the sole basis for the input catalogue. RAVE DR1, DR2, and DR3 were sourced from the original input catalogue (Kordopatis et al. 2013a).

The fourth data release, DR4 (Kordopatis et al. 2013a), incorporated observations drawn from a new input catalogue, using DENIS DR3 (DENIS Consortium 2005) as the basis, which had been cross-matched with the 2MASS point source catalogue (Skrutskie et al. 2006). The new input catalogue also extended the RAVE footprint to include lower Galactic latitudes ($5° < |b| < 25°$), where a colour cut using 2MASS photometry ($J - K > 0.5$ mag) was applied to preferentially select giants (Kordopatis et al. 2013a). This input catalogue is also used for the most recent data release (DR5; Kunder et al. 2017).

2.2 Target selection and observing strategy

Here we summarise the target selection and observing strategy described in the first data release (DR1, Steinmetz et al. 2006), as the selection function of a survey depends explicitly on how the observations are conducted.

From the input catalogue described in the previous section, 400 targets were selected for a given field of view. This selection was then split into two field files consisting of 200 stars each, to allow for two separate pointings. The 6dF instrument, used to conduct RAVE observations, consists of three fibre plates with 150 fibres each. These fibres were assigned to science targets according to a field configuration algorithm developed for the 2dF spectrograph (Lewis et al. 2002). However, for various reasons such as inaccessible areas on the fibre plate and fibre breakage, on average approximately 90 science fibres were allocated per pointing. Each observation consisted of a minimum of 3 (average 5) exposures, which were then stacked to improve the SNR per pointing. Figure 2 shows the distribution of fibres placed on science targets present in DR5 for all fields in the master list of RAVE field centres (see Sec. 4.1).

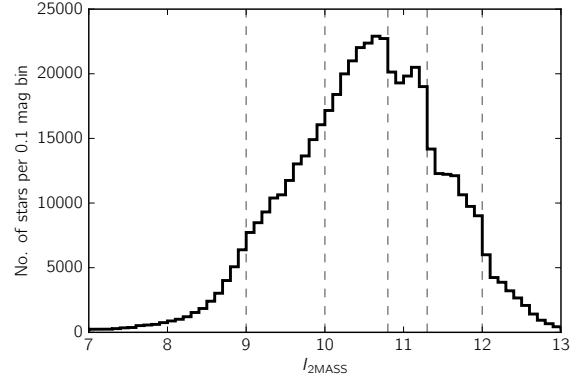During the first year and a half of observations, no

blocking filter was used on the spectrograph, so spectra were contaminated with second order diffraction (i.e., flux from the $\sim 4200 - 4400$Å wavelength range entered the primary wavelength range). Therefore, in DR5 the automated stellar parameter pipeline does not give stellar parameters for observations made before 6 April 2004.

A problem with fibre cross-talk due to bright ($I \sim 9$) stars adjacent to fainter stars was also identified in the period before DR1, and corrected for in the first iteration of the data reduction pipeline (Steinmetz et al. 2006). Therefore, in March 2006, the observing strategy was modified to observe stars only in a given magnitude bin for each pointing. These magnitude bins are illustrated in Figure 3 as vertical dashed lines. In addition to reduced fibre cross-talk, this change in the observing strategy had the added benefit of optimizing exposure times (e.g. bright fields could be observed in nominal conditions, while faint fields were preferentially observed when conditions were excellent), increasing the SNR per spectrum, and therefore resulting in more accurate stellar parameters. For fields in which interlopers or stars with variable brightness affected the fibres despite the magnitude selection, assessment and data reduction was conducted on a case-by-case basis to minimise the probability that problematic stars would enter the final catalogue.

2.3 Survey footprint

A simple footprint was imposed for observations: pointings were restricted to the Southern hemisphere and $|b| > 25°$. RAVE generally avoided regions on the sky with large extinction, i.e., close to the Galactic disc and towards the bulge. The primary reason for avoiding low Galactic latitudes was to prevent multiple stars entering a fibre, which had a spatial extent of $7''$ on the sky. Exceptions were a number of calibration fields around $|b| = 0°$ and several targeted observations of open clusters in the Galactic plane. In addition, there are a few fields in regions at the northern side of the bulge that originate from an interim input catalogue. We exclude these fields when evaluating the completeness of

RAVE, as the target selection in these fields differed from the general selection procedure.

In addition, we note the impact of utilizing DENIS DR3 as an input catalogue. The DENIS survey was observed in strips of $30°$ in declination and 12 arcmin in right ascension, with an overlap of 2 arcmin between consecutive strips. This observing pattern is embedded in the formulation of the selection function as a function of position (Eq. 1), and therefore is considered when evaluating both the completeness and selection function.

Figure 1 shows the adopted survey footprint for this study, which differs from the original footprint used for observations, as well as the distribution of individual stars in DR5.

2.4   RAVE Data Release 5

The latest public data release, DR5, contains information from $520\,781$ measurements of $457\,588$ individual stars. The distribution on the sky of these stars can be found in Figure 1. In addition to obtaining precise line-of-sight velocities V_{los} (typical uncertainties $\sim 2\,\mathrm{km\,s^{-1}}$), RAVE DR5 provides several other stellar parameters derived from the spectra: effective temperature (T_{eff}), surface gravity ($\log g$), an overall metallicity ([M/H]), and individual abundances for six elements: magnesium, aluminium, silicon, titanium, iron, and nickel.

Line-of-sight distances for RAVE stars have been estimated using a number of methods, including red-clump giants (e.g. Siebert et al. 2008; Veltz et al. 2008; Williams et al. 2013), isochrone fitting (e.g. Zwitter et al. 2010; Breddels et al. 2010), and a robust Bayesian analysis method described in Burnett & Binney (2010). RAVE DR5 provides distances derived using the method described in Binney et al. (2014), where stellar parameters, along with known positions, are used to derive spectrophotometric distance estimates for a large fraction of the stars in the survey.

In addition, Matijevič et al. (2012) performed a morphological classification of the spectra to allow for the identification of spectroscopic binaries and other peculiar stars in the catalogue. All targets in DR5 were also cross-matched with a number of other data sets: Tycho-2 (Høg et al. 2000), UCAC4 (Zacharias et al. 2013), PPMXL (Roeser et al. 2010), 2MASS (Cutri et al. 2003), WISE (Wright et al. 2010), APASS (Munari et al. 2014), and Gaia DR1 (Gaia Collaboration et al. 2016) to provide additional information such as proper motions, as well as apparent magnitudes in other filter passbands.

3   CATALOGUE DESCRIPTION AND QUALITY FLAGS

The RAVE survey was designed to have as simple a selection function as possible, to ensure that any biases could be accurately quantified. The initial target selection was based only on the apparent I-band magnitude ($9 \lesssim I \lesssim 12$) and sky position. An I-band selection was chosen as the most appropriate for efficient use of the spectral range of the 6dF instrument. In Figure 3 we show the distribution of I-band magnitudes in RAVE DR5. This distribution extends past the initial apparent magnitude limits due to uncertainties in

the SSS photometry used for the first input catalogue (see Figure 4 of Steinmetz et al. 2006). During 2006, the angular footprint was expanded to include regions close to the Galactic disc and bulge (Galactic latitude $5° < |b| < 25°$) as a result of the new input catalogue (see Section 2.1), and in these new regions a colour criterion ($J - K_s \geqslant 0.5$) was imposed to select for cool giant stars over more prevalent dwarfs (Kordopatis et al. 2013a). We can thus assume that the probability, S, of a star being observed by the RAVE survey is

$$S \propto S_{\mathrm{select}}(\alpha, \delta, I, J - K_s), \tag{1}$$

with α and δ denoting the equatorial coordinates of stars in a given region on the sky, within the defined footprint (see Figure 1).

Due to its complex history, and owing to observational constraints and actual atmospheric conditions on the respective day, the input catalogue for RAVE carries some inhomogeneity, and it is therefore not straightforward to construct a valid parent sample from this variety of data sets. However, one data set in particular, 2MASS, offers complete coverage of both the survey area and the magnitude range of RAVE. Therefore, we adopt the 2MASS photometry in order to compare our RAVE targets with as homogenous a sample as possible.

2MASS provides accurate J, H and K_s photometry for nearly all RAVE targets and, equally important, also for all other stars which could have potentially entered the input catalogue. Unfortunately, 2MASS does not provide I-band photometry, which is needed to construct our selection function (Eq. 1)[1], but we can compute an approximate I_{2MASS} magnitude via the following formula:

$$I_{\mathrm{2MASS}} - J = (J - K_s) + 0.2 \exp \frac{(J - K_s) - 1.2}{0.2} + 0.12 \tag{2}$$

Eq. 2 is derived by a direct comparison of 2MASS J and K_s magnitudes with DENIS I magnitudes. This transformation is determined by a polynomial fit in $I - J$ versus $J - K_s$, and is an evolution of Eq. 24 in Zwitter et al. (2008), with an improved fit for very cool stars. The distribution of I_{2MASS} magnitudes for RAVE DR5 is shown in Figure 3. Here, we find a significant number of RAVE stars which have $I_{\mathrm{2MASS}} < 9$. We note that this is due to the fact that both DENIS and SuperCOSMOS saturate around $I_{\mathrm{DENIS}} \sim 9$, and the conversion of their cross-matched 2MASS magnitudes gives magnitudes brighter than $I_{\mathrm{2MASS}} \sim 9$.

In addition, there are a number of other factors which also have an influence on the final selection function, which we will describe in the following sections.

3.1   Sample selection

3.1.1   RAVE quality criteria

To asses the completeness S_{select} (Eq. 4), we remove fields which were reprocessed during the course of data reduction

---

[1] Recently, data from the APASS survey (Munari et al. 2014) became available which provides SDSS i magnitudes, but this survey also suffers some saturation problems for bright stars. Currently, APASS is being extended to brighter magnitudes, so in the future this could be a valuable alternative to 2MASS.

Table 1. Quality criteria for the 2MASS parent sample.

Criterion	Requirement	Description
$\texttt{ph\_flag}_J$	A,B,C or D	good J-photometry
$\texttt{ph\_flag}_{K_s}$	A,B,C or D	good K_s-photometry
$\texttt{cc\_flag}_J$	0	no artifact/confusion
$\texttt{cc\_flag}_{K_s}$	0	no artifact/confusion
$\texttt{gal\_contam}$	0	not contaminated by extended source
$\texttt{pm\_flag}$	0	not associated with asteroid/comet

(indicated in DR5 with either 'a','b', or 'c' appended to the $\texttt{RAVE\_OBS\_ID}$). After removing these stars, we are left with a sample of 518 079 entries in DR5, corresponding to 455 626 individual spectra.

3.1.2   2MASS quality criteria

We compute an $I_{\rm 2MASS}$ value (Eq. 2) for each 2MASS star and clean the data from spurious measurements. Our requirements for a 'valid' measurement are given in Table 1.

4   THE SELECTION FUNCTION

4.1   Field-by-field

We first consider the selection function of RAVE on a field-by-field basis, in order to account for changes in the observing strategy as a function of time.

First, the observation date and position for each individual pointing is identified from a master list of RAVE field centres and their corresponding given $\texttt{RAVE\_OBS\_ID}$. In order to make the most accurate comparison between RAVE and our parent 2MASS sample, we must utilize accurate field centre positions. We identify 6593 individual pointings from this master list, corresponding to 1598 unique field centres. Next, we compare this list with a table containing information about the placement of fibres for each pointing. For each pointing, we count the number of fibres placed on science targets, as well as how many fibres were assigned to the sky, or simply not used. As shown in Figure 2, out of the 150 available fibres on 6dF, at maximum approximately 130 fibres were placed per field pointing, with an average of approximately 90 fibres per RAVE pointing. From the fibres placed on science targets, we then consider how many of these observations obtained spectra for which stellar parameters are published in DR5, and characterize the $I_{\rm 2MASS}$ distribution by counting the number of stars per 0.1 dex magnitude bin. Then, for each RAVE pointing we determine the number of 2MASS stars available in each magnitude bin, with the quality criteria described in Sec. 3.1.2 applied. For the final table (Table 2), we include only those fields which have stars parametrized and published in DR5.

An excerpt of the resulting completeness fraction on a field-by-field basis can be found in Table 2. The completeness fraction for a field centered on (α, δ) is given by

$$S_{\rm select}({\rm field}_{\alpha,\delta}) = \frac{\sum\sum {\rm N_{RAVE}}({\rm field}_{\alpha,\delta}, {\rm I, J-K_s})}{\sum\sum {\rm N_{2MASS}}({\rm field}_{\alpha,\delta}, {\rm I, J-K_s})}, \qquad (3)$$

where the double sum is over a given $I_{\rm 2MASS}$ range and the total $J - K_s$ range in that field.

It is important to note that there exists substantial overlap between RAVE pointings, and therefore it is not appropriate to combine the data given in Table 2 to construct a selection function for the entire RAVE survey. In order to facilitate this, we must consider the completeness of RAVE for equal, discrete areas on the sky. We do note however, that on scales below the size of the field plate ($\simeq 28.3\,{\rm deg}^2$), we expect inhomogeneities due to certain technical constraints with fibre positioning on the field plates used for RAVE observations (see Figure 3 of Steinmetz et al. 2006).

4.2   Equal area on the sky (healpix)

To construct our parent RAVE sample for considering equal areas on the sky, we first remove all repeat observations and keep for each star only the observation with the highest SNR. This is in contrast to Section 4.1, where we do not remove duplicates. Here, the goal is not to conserve the temporal information, but to accurately reconstruct the sky coverage and completeness of RAVE, so any given star is counted only once, even if it was observed multiple times. In addition, for the rest of the study we will only consider stars within the adopted footprint (Fig. 1). This excludes ~ 7000 stars available in RAVE DR5. These specific stars are documented in the RAVE DR5 catalogue with $\texttt{FootPrint\_Flag}$.

We then divide the sky into equal area pixels using the HEALPIX algorithm (Górski et al. 2005). As described in the previous section, using the RAVE fields directly would cause additional complications for certain applications because some fields are overlapping. We use 12 288 pixels for the whole sky (NSIDE = 32) which results in a pixel area of $\simeq 3.36\,{\rm deg}^2$, much smaller than the size of a RAVE field ($\simeq 28.3\,{\rm deg}^2$). We note that we use the 'nested'[2] scheme and equatorial coordinates (α, δ) to determine the corresponding pixel ID for any given star. We count the number of RAVE stars, $N_{\rm RAVE}$, in each pixel (centered on α and δ) as a function of $I_{\rm 2MASS}$ in 0.1 dex magnitude bins. To estimate the completeness we follow the same procedure for all stars in our 2MASS sample to obtain $N_{\rm 2MASS}$ and then compute

$$S_{\rm select}({\rm pixel}_{\alpha,\delta}) = \frac{\sum\sum {\rm N_{RAVE}}({\rm pixel}_{\alpha,\delta}, {\rm I, J-K_s})}{\sum\sum {\rm N_{2MASS}}({\rm pixel}_{\alpha,\delta}, {\rm I, J-K_s})}, \qquad (4)$$

where the double sum is over a given $I_{\rm 2MASS}$ range and the total $J - K_s$ range in that pixel. Table 3 gives an excerpt of the completeness fraction for HEALPIX pixels, in 0.1 magnitude width bins. Full versions of Tables 2 and 3 are available as part of the online-only materials, and also via the RAVE website.

The resulting completeness as a function of magnitude and sky position has already been shown in the fourth RAVE data release paper (Figure 3 of Kordopatis et al. 2013a),

---

[2] The nested, or tree structure, scheme refers to the way that HEALPIX pixels are numbered (see Figure 4 of Górski et al. 2005). The hierarchical structure of the nested scheme allows for degrading the resolution of a HEALPIX map from the base resolution, and is the same scheme used for Gaia DR1.

Table 2. Completeness fraction of RAVE on a field-by-field basis, for 0.1 mag width bins.

RAVE Field Index	Field Center (α, δ)	Observation Date YYYYMMDD	Fibres Placed N	Spectra N	2MASS N	0.0	...	9.9	10.0	10.1	...	14.0
								Completeness Fraction ($I_{2\mathrm{MASS}}$)				
0	(143.20, -8.75)	20030412	124	121	14170	-		0.0	0.0	0.0		0.00017
⋮												
1077	(181.67, -7.27)	20060418	93	93	7915	-		0.333	0.391	0.273		0.0
1078	(209.60, -26.43)	20060418	96	96	16382	-		0.167	0.156	0.156		0.0
⋮												
6430	(222.48, -44.90)	20130404	86	85	69564	-		0.0	0.0	0.0		0.0

Table 3. Completeness fraction of RAVE on a pixel-by-pixel basis, for 0.1 mag width bins. Here, the nested scheme is used to determine a given pixel ID.

HEALPIX Pixel ID Index (Nested)	0.0	...	9.9	10.0	10.1	...	14.0
			Completeness Fraction ($I_{2\mathrm{MASS}}$)				
0	-		0.200	0.667	0.600		0.0
⋮							
10000	-		0.250	0.462	0.500		0.0
10001	-		0.571	0.500	0.250		0.0
⋮							
12287	-		0.333	0.333	0.600		0.0
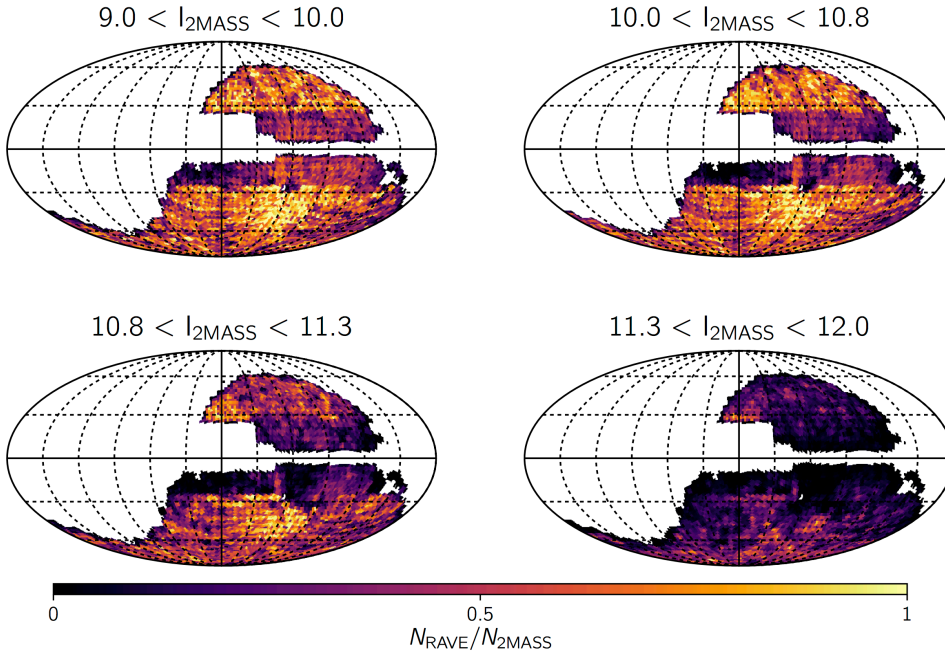
Figure 4. Completeness of RAVE DR5 in Galactic coordinates as a function of observed magnitude bins (compare with similar plot for completeness fraction of DR4, Figure 3 of Kordopatis et al. 2013a). The HEALPIX pixels are colour-coded by the fractional completeness, ($N_{\mathrm{RAVE}}/N_{2\mathrm{MASS}}$).
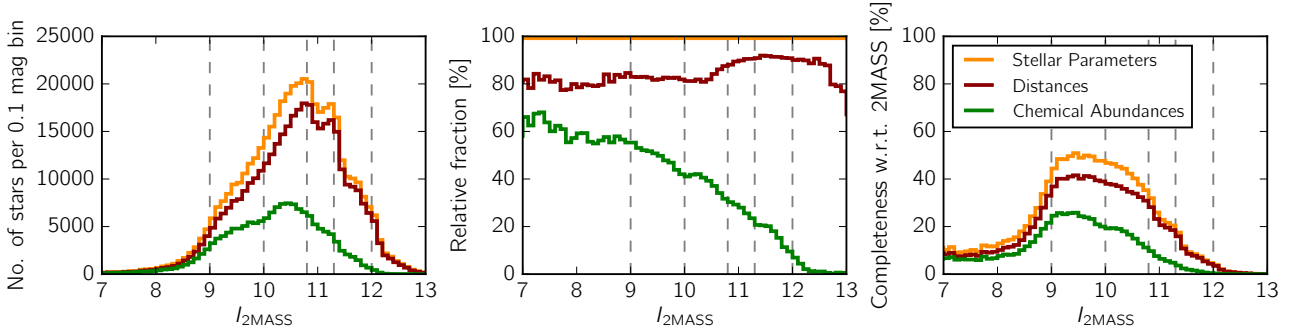
Figure 5. *Left:* Histogram of stellar parameters, chemical abundances, and distance measurements in RAVE DR5 which satisfy the quality criteria and parameter limits given in Section 4.3, as a function of magnitude (S_{pipeline}, Eq. 6). Stars with stellar parameters are indicated in orange, distances in red, and chemical abundances in green. Observed magnitude bins are indicated with dashed lines. *Middle:* relative fraction of stars with derived parameters as a function of magnitude. We use radial velocity as a baseline for comparison, as all stars satisfying the criteria given in Section 4.3 have radial velocity measurements. As all stars with radial velocities in this sample also have stellar parameters, the completeness of stellar parameters is 100 per cent. *Right:* completeness fraction of derived parameters, relative to the number of 2MASS stars, as a function of magnitude. This represents the complete selection function with respect to 2MASS (see Eq. 7).
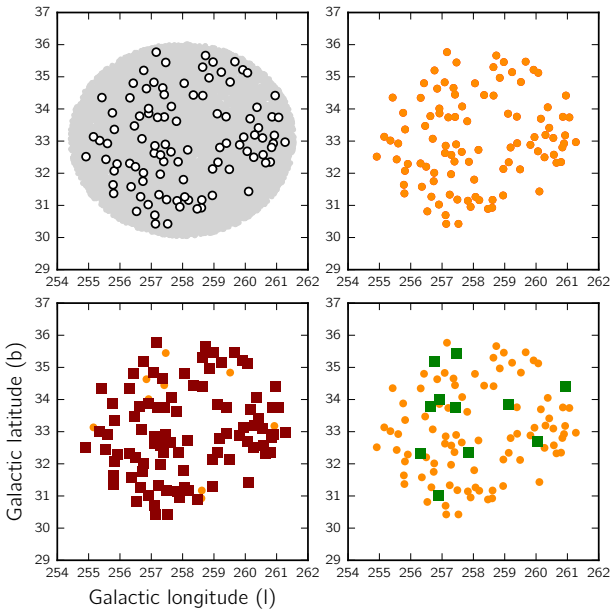
Figure 6. Distribution of RAVE stars (open circles) and 2MASS (grey) stars on the sky, for a given RAVE pointing. Orange indicates that a given RAVE star has spectral parameters from the spectral parameter pipeline (T_{eff}, $\log g$, [M/H]), red squares indicate stars which have distance estimates from the distance pipeline, and green squares indicate stars which have all abundance measurements from the chemical abundance pipeline.

and we replicate it here for DR5 in Figure 4[3]. Overall, as in DR4, we find the completeness is highly anisotropic on the sky for any given magnitude bin, and drops off significantly for fainter magnitudes.

---

[3] We note that the completeness fraction can, in some very rare cases, be null or greater than one. This is due to the fact that we remove stars from our parent 2MASS sample that do not meet the specified quality criteria.

4.3 Impact of the analysis pipeline

Until now we have only investigated effects that originate from the RAVE target selection. However, when considering certain applications, there is another important issue: namely, the effects of the automated pipelines. RAVE DR5 contains output from a number of pipelines which provide additional information for observed stars. As described in Sec. 2, in addition to line-of-sight velocities, RAVE provides estimates of stellar parameters such as effective temperature, surface gravity, elemental abundances, as well as distance and age estimates.

Here we consider the completeness fraction of stars with assigned stellar parameters from the stellar parameter pipeline, following the recommendations given by Kordopatis et al. (2013a), selecting all stars that have

- SNR $\geqslant 20$,
- $|\texttt{correctionRV}| < 10\,\mathrm{km\,s}^{-1}$,
- $\sigma(V_{\mathrm{los}}) < 8\,\mathrm{km\,s}^{-1}$,
- $\texttt{correlationCoeff} > 10$ (Tonry & Davis (1979) correlation coefficient).

In addition, this pipeline yields reliable results only in a restricted region in stellar parameter space (Kordopatis et al. 2013a). We explicitly implement this by using only stars with

$$
\begin{aligned}
4000\mathrm{K} &< T_{\mathrm{eff}} < 8000\mathrm{K}, \\
0.5 &< \log g < 5.
\end{aligned}
\tag{5}
$$

These limits are based on the range of parameters for the spectra used for the learning grid of the analysis pipeline (Kordopatis et al. 2011, 2013a), as well as unphysical or highly unlikely combinations of derived parameters.

These restrictions have to be taken into account when comparing observed data with specific Galaxy models. They can be expressed as an additional selection function

$$
S_{\mathrm{pipeline}} = S_{\mathrm{pipeline}}(T_{\mathrm{eff}}, \log g, [\mathrm{Fe/H}])
\tag{6}
$$

and hence the complete selection function S is

$$
S = S_{\mathrm{pipeline}} \times S_{\mathrm{select}}.
\tag{7}
$$

We give examples of this effect in Figures 5 and 6, for the selection function evaluated with HEALPIX pixels, and field-by-field, respectively. Figure 5 shows the distribution of the number of stars satisfying these criteria that have derived parameters (stellar parameters, distance, and chemical abundances) available in RAVE DR5 as a function of $I_{2\mathrm{MASS}}$ magnitude (left and middle panels represent S_{pipeline}, see Eq. 6), as well as the completeness fraction of these parameters in RAVE with respect to 2MASS (right panel represents the complete selection function, see Eq. 7). We find that the number of stars having a given parameter in DR5 varies as a function of magnitude, with the brightest magnitude bin ($9 < I_{2\mathrm{MASS}} < 10$) having the highest number of stars with stellar parameters, distances, and chemical abundances. When we consider the relative fraction of stars with a given parameter (using radial velocity as a baseline, as all stars satisfying the quality criteria have radial velocity measurements), we find stellar parameters are derived for all stars with radial velocities, while distances are derived for ~ 80 per cent of these stars. The relative fraction of stars with chemical abundance estimates is calculated for stars which have all six element abundances derived from the chemical abundance pipeline (Boeche et al. 2011). We find that $\sim 40 - 60$ per cent of stars brighter than 10th magnitude have chemical abundance information available in DR5. Finally, when we consider the completeness of a given derived parameter in RAVE with respect to 2MASS, we find that stars in the brightest magnitude bin ($9 < I_{2\mathrm{MASS}} < 10$) have the highest completeness. This panel represents the complete selection function (see Eq. 7).

In Figure 6, we characterize the completeness fraction of derived parameters for a typical RAVE pointing. RAVE stars are shown in black, purple, and orange, with the underlying 2MASS parent sample shown in grey. For this particular pointing, we find all stars have estimated stellar parameters, ~ 90 per cent have distances, and ~ 10 per cent have chemical abundance estimates.

5   COMPARISON WITH A GALACTIC MODEL

We now explore the potential influence of the selection function with respect to inducing biases in the stellar parameter distributions of our RAVE DR5 stars compared with what we expect from models of the Galaxy. For this comparison, we utilize the stellar population synthesis code GALAXIA[4] (Sharma et al. 2011).

GALAXIA is a tool which uses a given Galactic model to conduct synthetic observations, generating a catalogue which imitates any given survey of the Milky Way. Here, we use the default provided in GALAXIA, a modified version of the Besançon model (Robin et al. 2003). Details on the extent of these modifications can be found in Sharma et al. (2011). The Besançon model within the GALAXIA framework has been found to agree quite well with Besançon star counts (Sharma et al. 2011). The input parameters for GALAXIA are very simple, and correspond well to our adopted form of RAVE's selection function (Eq. 1).

The catalogue may be generated for a given circular

area on the sky, as well as for the whole sky. In order to compare these mock observations with our two methods of characterising the selection function of RAVE, we generate two catalogues: one on a field-by-field basis, and one full-sky, which is then divided into HEALPIX pixels. For each of these catalogues, we allow GALAXIA to generate stars with apparent I-band magnitude $0 < I < 13$, and no colour restriction. We then perturb the output from GALAXIA with a simple noise model to imitate observational uncertainties present in RAVE, and apply the RAVE selection function. We refer to this modified catalogue as our 'mock-RAVE' catalogue. The mock-RAVE catalogue can then be compared to our parent Galaxia sample (where the RAVE selection function has not been applied), to evaluate the effect that the selection function has on fundamental distributions such as kinematics and chemistry.

5.1   Applying uncertainties to generate a mock-RAVE catalogue

GALAXIA provides stellar parameters and magnitudes with infinite precision and accuracy. This does not reflect our observational data, where each of the derived parameters has intrinsic uncertainties associated with its measurements. In order to facilitate an accurate comparison between the mock catalogue and real RAVE data, we perturb J, K_s, T_{eff}, $\log g$, and [Fe/H] available in our GALAXIA catalogue based on the uncertainty distributions of 2MASS magnitudes and RAVE stellar parameters before applying the selection function of RAVE. We then apply the selection function of RAVE using both methods described in Sec. 4: field-by-field and HEALPIX pixels. In addition to scattering the GALAXIA distributions with our simple noise model, we slightly modify the metallicity distribution of the thick disc and the halo of our GALAXIA output, for better agreement with observations.

5.1.1   2MASS apparent magnitude uncertainties

First, we modify the output GALAXIA 2MASS J and K_s magnitudes by a simple noise model, derived from the observational uncertainties in 2MASS. To do this, we characterize the observational uncertainty for a given 0.1 magnitude bin as a function of magnitude. We model the distribution of uncertainties in each bin as a Gaussian, and draw from this Gaussian to obtain an 'observational uncertainty' on our GALAXIA output. Typical 2MASS J magnitude uncertainties are of the order of 0.025 dex. From the modified J and K_s values, we obtain an $I_{2\mathrm{MASS}}$ for each GALAXIA star using Eq. 2.

5.1.2   Applying RAVE-like uncertainties to stellar parameters

In order to compare the stellar parameters available in this mock catalogue with those derived from the RAVE DR5 stellar parameter pipeline, we must first modify the output from GALAXIA with the uncertainty distributions of RAVE stellar parameters. The RAVE DR5 stellar parameter pipeline provides individual uncertainties for each star, and we can use the distribution of these uncertainties to modify our initial GALAXIA catalogue by RAVE-like uncertainties, similar
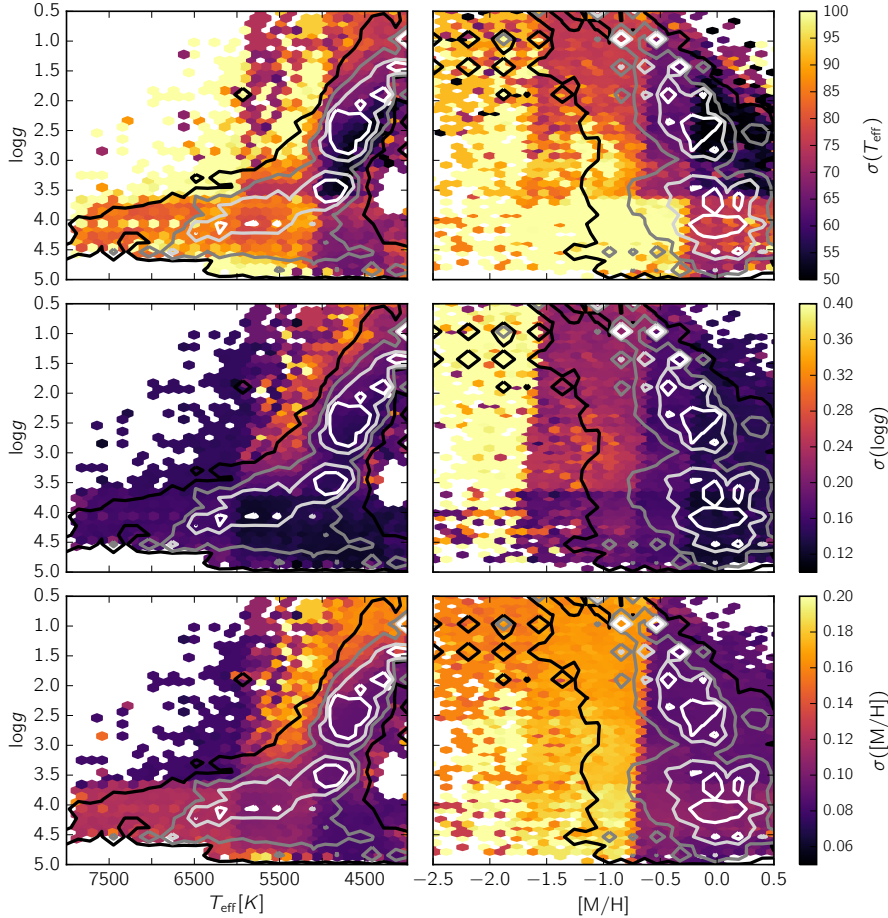
---

[4] http://galaxia.sourceforge.net/

Figure 7. Mean uncertainties as a function of stellar parameters available in RAVE DR5. The left column shows the distribution of uncertainties in $T_{\rm eff}$- $\log g$ space, and the right column shows the same but in [M/H]-$\log g$ space. Each row shows the distribution of the uncertainties of a different parameter as indicated by the colour bars on the far right. The contours indicate 33, 67, 90, and 99 per cent of all RAVE DR5 stars.

to the process used in the previous section, but in a higher-dimensional space due to correlations between the uncertainties.

In Figure 7, we show the correlation of uncertainties as a function of position in different planes of stellar parameters. Here, we colour-code the mean uncertainty as a function of the stellar parameters in $T_{\rm eff}$- $\log g$ and $T_{\rm eff}$-[M/H] space. The highest uncertainties are found primarily in hot, giant stars in the $T_{\rm eff}$- $\log g$ plane, and metal-poor stars in the [M/H]-$\log g$ plane (see also Table 4, Kunder et al. 2017). However, comparing these regions to the density contours, we find that these regions are sparsely populated, and therefore should not significantly affect the mean uncertainty. The abrupt jumps, visible at e.g. $T_{\rm eff} \sim 5000$ K and [M/H] ~ -0.7, result from discrete coverage of the stellar parameter space by model atmospheres that are compared to the observed spectra by the pipeline. We find that the majority of RAVE stars have similar uncertainties in spectral parameters, with $\langle\sigma(T_{\rm eff})\rangle \sim 50 - 75$ K, $\langle\sigma(\log g)\rangle \sim 0.1 - 0.2$ dex, and $\langle\sigma([{\rm M/H}])\rangle \sim 0.1$ dex.

In addition to an anisotropic distribution of uncertainties in in $T_{\rm eff}$- $\log g$ and $T_{\rm eff}$-[M/H] space, it has been well documented that these uncertainties in the derived atmospheric parameters are also correlated (see Figure 6 of Ko-

rdopatis et al. (2011) and Figure 23 of Kordopatis et al. 2013a). Due to these correlations, it is not sufficient to simply model the uncertainties as individual Gaussians and draw from them. Instead, we consider the distribution of uncertainties to have the form of a multivariate Gaussian, and estimate the covariance between uncertainties in $T_{\rm eff}, \log g$, and [M/H]. We then draw from this multivariate Gaussian to obtain simultaneously uncertainties for these three respective parameters. Note that in this way we can introduce only the internal uncertainties of the analysis pipeline, but not systematic shifts coming from inaccuracies of the stellar atmosphere models.

Finally, we apply $S_{\rm pipeline}$ by setting weights to zero for all stars that do not fulfill the criteria given in Eq. 5. We refer to the result as the mock-RAVE catalogue. The effect of this step is model dependent as, for example, the number of super-solar metallicity stars varies between different Galaxy models. Using the version of the Besançon model in Galaxia, we find that approximately 9 per cent of stars fall outside of our $T_{\rm eff}$ and $\log g$ limits.

The effect of applying these observational uncertainties as well as $S_{\rm pipeline}$ is shown in Figure 8. The top row shows 2D histograms of stellar parameters for our Galaxia sample (without the application of $S_{\rm pipeline}$). RAVE-like uncer-
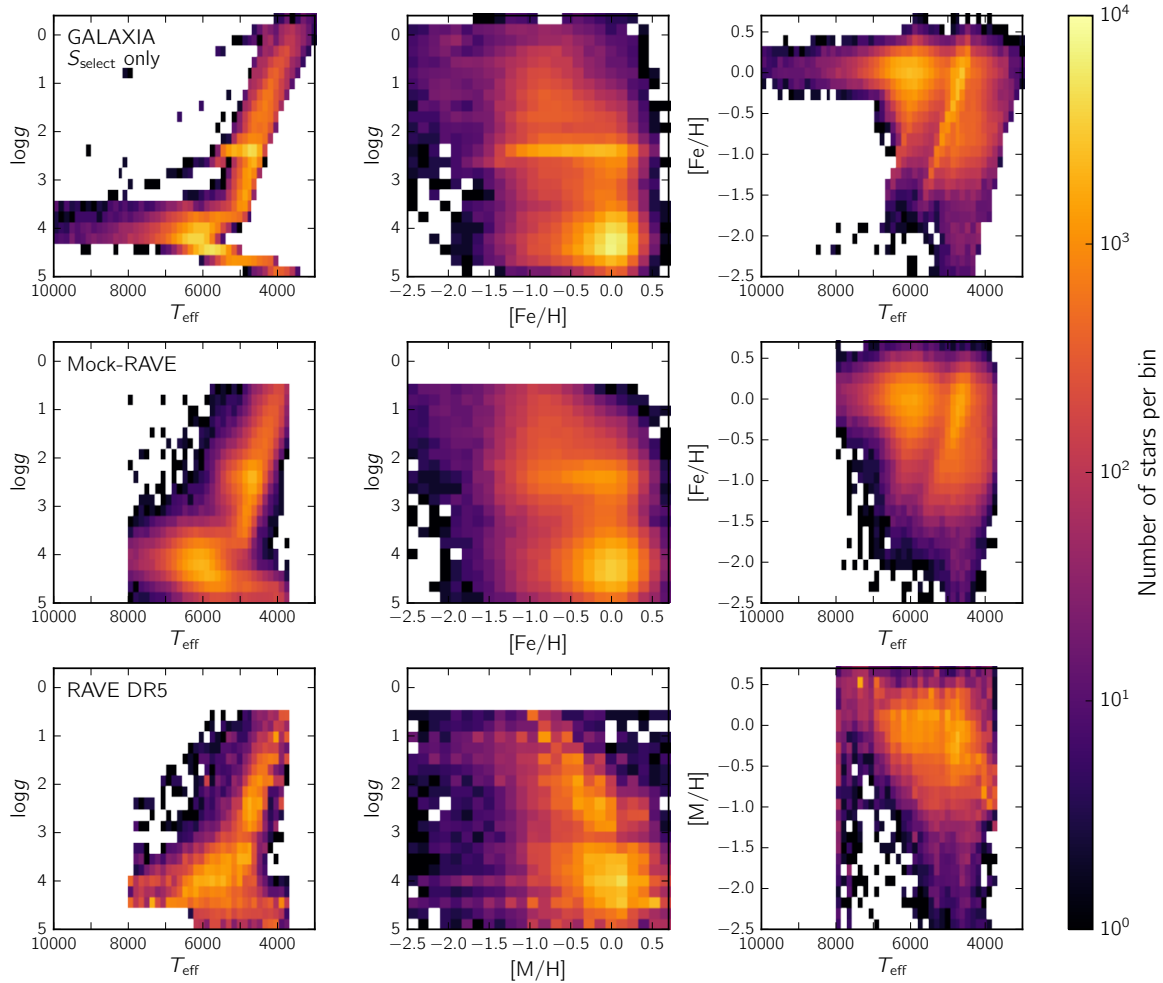
Figure 8. 2D histograms of three stellar parameter spaces: $\log g$-$T_{\rm eff}$ (left), $\log g$-abundance ([Fe/H] for GALAXIA, [M/H] for RAVE) (middle), and abundance-$T_{\rm eff}$ (right). The top row shows these 2D histograms for our GALAXIA sample with the RAVE selection function applied. In the middle row we show our GALAXIA sample which has had both the RAVE selection function and RAVE-like uncertainties applied. The bottom row shows our RAVE DR5 sample. The colour scale is log normalized.

tainties and the selection function are applied to obtain the panels in the middle row. Our RAVE sample is shown on the bottom row. Overall, we find good agreement in the distribution of these stellar parameters between the observations and the mock-RAVE catalogue.

5.2   Impact of the selection function

We now turn to the implications of the observed stellar populations due to the selection function of RAVE. While RAVE targets within the footprint were selected on purely photometric grounds, it remains to be seen if changes to the observing strategy as well as the applied colour cut at low latitudes have induced biases in the observed characteristics of the sample. In order to test if RAVE is a kinematically unbiased survey, we compare the Galactocentric cylindrical velocity distributions of the parent GALAXIA sample with those of the mock-RAVE catalogue. We also examine potential biases in the metallicity distribution of the sample, as abundance measurements are highly correlated with other derived values, such as effective temperature and surface

gravity, as well as external characteristics such as kinematics. Hence, biases in either velocity or metallicity are potentially harmful if undetected, for both chemical evolution and dynamical modeling.

We take a uniformly selected subsample of our full GALAXIA catalogue in the footprint of RAVE as our expected 'parent' sample (i.e., what we consider to be the 'truth' for the purpose of this exercise), and compare it to our mock-RAVE catalogue. Any considerable deviations between the two distributions may indicate a bias in RAVE due to the selection function. We note that for this exercise, we do not apply RAVE-like uncertainties to the velocities or metallicities in our mock-RAVE catalogue (i.e., here we use the true GALAXIA output). In addition to a GALAXIA subsample limited to $I < 13$, we also investigate the effects of limiting our GALAXIA subsample to $I < 12$, as it has been shown in Figure 3 that RAVE is not complete at $I_{\rm 2MASS} = 13$. Quantitatively, in order to characterize the skewness of each distribution we compute quartile values (Q_1, Q_2, Q_3), which represent the 25$^{\rm th}$, 50$^{\rm th}$, and 75$^{\rm th}$ percentiles, respectively.
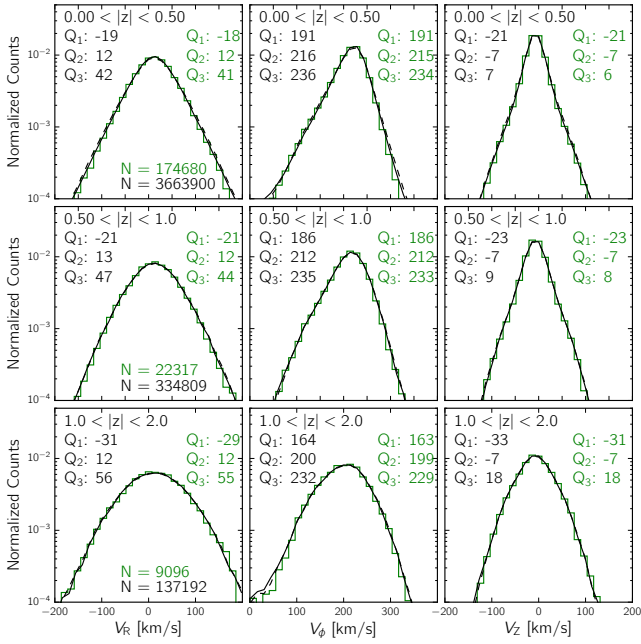
Figure 9. Distributions of Galactocentric cylindrical velocity components for samples of giant stars ($\log g < 3.5$) at different distances from the Galactic plane as indicated in the panels. The green histograms show the velocity distributions in the mock-RAVE catalogue, while the black-dashed curves show the distributions for our parent GALAXIA subsample of giants. Solid black curves show the distribution for a parent GALAXIA sample limited to $I < 12$. Quantile values (Q_1, Q_2, Q_3) for both distributions are given in each panel, which represent the 25th, 50th, and 75th percentiles, respectively. The sample size (N) for the distributions are shown in green and black, representing the mock-RAVE sample and the parent Galaxia sample limited to $I < 12$, respectively. The y-axis is plotted on a logarithmic scale.

5.2.1 *Velocity distribution comparison*

We first examine the effect of our selection function on distributions of the cylindrical Galactocentric velocity components in our mock-RAVE catalogue. Our results are shown in Figures 9, 10, and 11, with the GALAXIA distribution shown as dashed black curves, and the mock-RAVE catalogue shown in green. A GALAXIA distribution limited to $I < 12$ is shown as solid black curves. Quantile values are given in each panel.

For our giant and main sequence region samples (Figures 9 and 10), we find nearly identical distributions for all
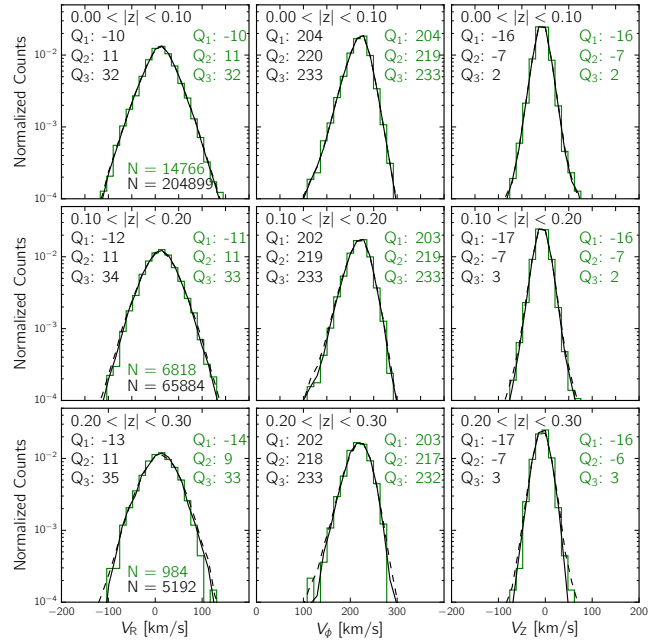
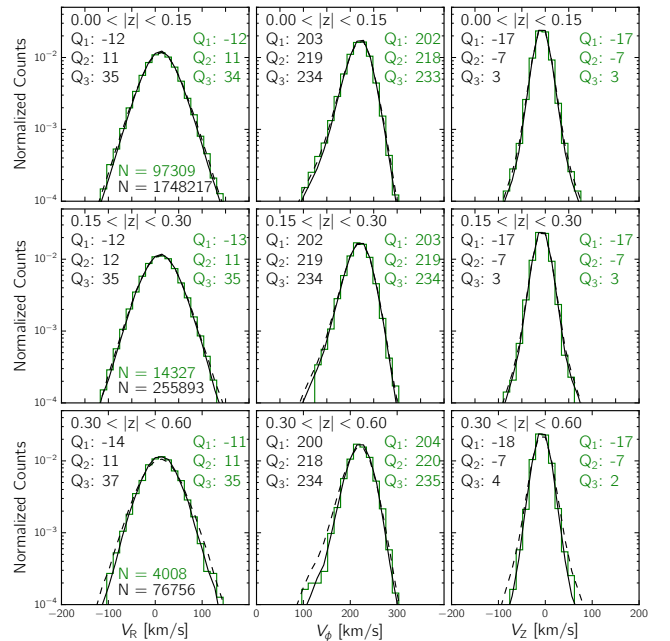**Figure 10.** Same as Figure 9 but for the main sequence region ($\log g > 4.0, T_{\rm eff} < 5500$K) sample.

Figure 11. Same as Figure 9 but for the turnoff region ($\log g > 3.5, 5500\,{\rm K} < T_{\rm eff} < 7000\,{\rm K}$) sample.

distance bins when comparing our mock-RAVE catalogue with the respective parent GALAXIA distributions. We consider the distributions to agree if we find all three quartiles to agree within $5\,{\rm km\,s^{-1}}$. Using this criterion, we confirm that the selection function does not impose kinematic biases for these populations as a whole. We note that when we consider only low-latitude fields ($5° < |b| < 25°$), the

colour criterion that was imposed to select preferentially for giants (see Section 3.1.1) reflects to a small bias in age. Further comparisons with the model have shown that this age bias does not introduce a significant kinematic bias, however, we urge some caution when considering the velocity distributions for these low-latitude fields.

We also find good agreement in most height bins for each velocity component of our turnoff region sample (Figure 11). However, for the most distant bin ($0.30 < |z| < 0.60$ kpc), there is a slight difference between the distributions in the low-V_ϕ tail. Specifically, the application of the selection function leads to an underrepresentation of stars with $V_\phi \lesssim 150\,\mathrm{km\,s^{-1}}$ in our mock-RAVE catalogue. Bias is present in all components of the velocity, but we find it most clearly in V_ϕ, as the velocity distribution functions for the thin disc, thick disc, and halo do not have the same mean for this component.

The difference that we find can be explained by the difference in magnitude distributions between our two samples: our parent GALAXIA sample extends to $I_{2\mathrm{MASS}} \sim 13$ (see Section 5), whereas our mock-RAVE sample follows the I-magnitude distribution of RAVE (see Figure 3), by the definition of the selection function. As a consequence, there are relatively few stars observed in RAVE with $12 < I < 13$ compared to those present in our parent GALAXIA sample. By having a larger fraction of stars at fainter magnitudes, the parent GALAXIA sample probes more of the thick disc and halo compared to our mock-RAVE sample. This effect also is reflected in differences that we see between the metallicity distributions (see Section 5.2.2 and Figure 12). This discrepancy is small (and indeed disappears if we limit our parent GALAXIA sample to $I_{2\mathrm{MASS}} < 12$), and overall the distributions meet our criterion (all three quartiles agree within $5\,\mathrm{km\,s^{-1}}$), so we consider the turnoff region stars to also be kinematically unbiased.

Similar tests were done for a sample of hot dwarf stars ($\log g > 3.5, T_\mathrm{eff} > 7000\mathrm{K}$), but are not shown here. As with the our turnoff region sample, we find our sample of hot dwarfs to also be unbiased for $I < 12$.

5.2.2 *Metallicity distribution comparison*

Next, we examine the metallicity distributions of the GALAXIA samples and our mock-RAVE catalogue. The metallicity distributions for each subsample in different slices in distance $|z|$ from the Galactic plane are shown in Figure 12. Here, we consider the distributions to agree if all three quartiles agree within 0.1 dex.

For giants (left column of Figure 12) and stars in the main sequence region (middle column of Figure 12), we find very good agreement between the GALAXIA and mock-RAVE metallicity distributions for all distance bins. For stars in the main sequence region and the most distant bin ($0.20 < |z| < 0.30$ kpc), we find that in our mock-RAVE sample the metal-poor tail of the metallicity distribution is slightly underrepresented, compared to the GALAXIA sample. However, this difference can be explained by small number statistics, as our mock-RAVE sample would need only one star below $[\mathrm{M/H}] \sim -0.6$ to reconcile the difference between the two distributions. Again, despite this small discrepancy, the quartile values satisfy our criterion, and therefore we consider our main sequence region sample to be
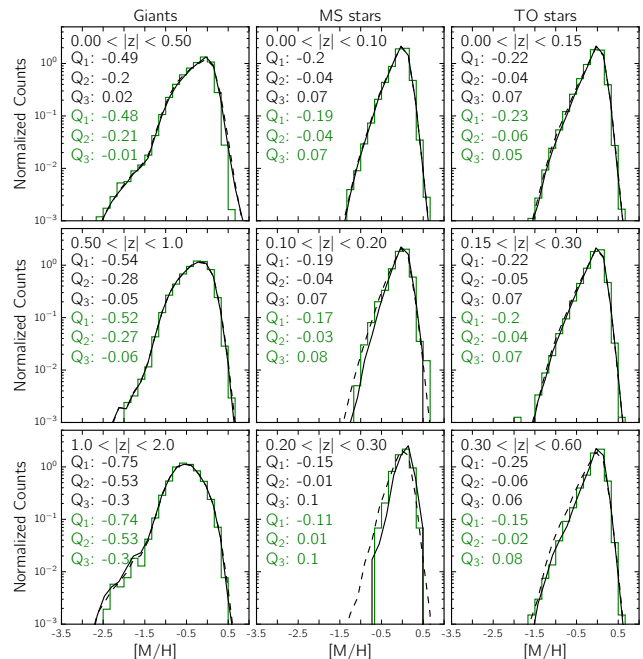

Figure 12. Metallicity distributions for each sample in different distances from the Galactic plane as indicated in the panels. The left column shows the distributions for giants, the middle shows main sequence region stars, and the right shows turnoff region stars. The black-dashed curves indicate the underlying distributions for our GALAXIA parent sample, while the green histograms show the metallicity distributions in the mock-RAVE catalogue. Solid black curves show the distribution for a parent GALAXIA sample limited to $I < 12$. Quartile values (Q_1, Q_2, Q_3) for both distributions are given in each panel. The y-axis is plotted on a logarithmic scale.

chemically unbiased. We conclude that for giants and stars in the main sequence region, our metallicity distribution is minimally affected by our selection function.

Similarly, for the turnoff region sample (right column of Figure 12), we find good agreement for the two closest distance bins, with differences between the two distributions found only in the furthest distance bin ($0.30 < |z| < 0.60$ kpc). For this bin, we find that our criterion is barely met, with Q_1 differing by ~ 0.1 dex. This discrepancy between the two distributions is explained by the difference in magnitude limits as described in Section 5.2.1. That is, as our parent GALAXIA sample includes a larger fraction of faint ($12 < I < 13$) stars compared to our mock-RAVE sample, it probes a larger volume, and therefore more of the thick disc and halo. This effect is less prominent for our giant sample, as the relative fractional increase of thick disc and halo stars is much less for giants, compared to our dwarf sample. We conclude that our turnoff region sample is unbiased for $I_{2\mathrm{MASS}} < 12$. As with the velocity comparisons, we also test the $[\mathrm{M/H}]$ distributions for a sample of hot dwarf stars ($\log g > 3.5, T_\mathrm{eff} > 7000\mathrm{K}$), and find them to also be chemically unbiased.

6 DISCUSSION AND CONCLUSIONS

We have described, in detail, how to evaluate the selection function S of the RAVE survey in two different ways: field-by-field, and HEALPIX pixels. In addition, we discussed the uncertainty distributions of RAVE DR5 and illustrated that these uncertainties depend heavily on the position in stellar parameter space. We then generated a mock-RAVE catalogue by applying the detailed selection function to the model output, and modified the raw GALAXIA output by RAVE-like uncertainties.

To investigate that RAVE is a kinematically and chemically unbiased survey, we tested the impact of S on the resulting velocity and metallicity distributions using a modified version of the Besançon model available in the GALAXIA framework. The velocity and metallicity distributions of our mock-RAVE catalogue were compared with the distributions of the underlying GALAXIA populations. We find that, for $I < 12$, our selection function does not intrinsically induce biases in the kinematics or chemistry of stars within the stellar parameter space covered in RAVE (4000K $< T_{eff} <$ 8000K and $0.5 < \log g < 5.0$), with respect to expectations from the Besançon model available in Galaxia. We do find some small biases when we consider a parent sample extending to $I = 13$, however, it has been shown that the completeness of RAVE falls off for fainter magnitudes (due to the magnitude limit imposed from the input catalogues), and therefore our conclusion stands for the magnitude range where we consider RAVE to provide a representative sample of stars ($9 < I < 12$). Under these criteria, and within this parameter space, RAVE stars provide unbiased samples in terms of kinematics and metallicities that are well suited for kinematic modeling without taking into account the detailed selection function via volume corrections.

For our giant and main sequence region samples, we find good agreement between the parent GALAXIA sample and our mock-RAVE catalogue. We find similar trends for our sample of turnoff region stars, with small differences in the velocity distributions for the most distant stars, and the metal-poor tail of the [M/H] distribution. However, we explain this bias due to the fact that our GALAXIA sample includes a larger number of stars at fainter magnitudes compared to our mock-RAVE catalogue. The parent GALAXIA sample therefore probes a larger volume than our mock-RAVE catalogue, and consequently more of the thick disc and halo populations. As we are able to account for the source of these differences, we consider our turnoff region sample to also be kinematically and chemically unbiased for $I_{2MASS} < 12$.

Recently, a number of studies used RAVE data, and in particular subsamples of giant stars, for kinematic modeling (e.g. Binney et al. 2014; Piffl et al. 2014; Minchev et al. 2014; Williams et al. 2013; Kordopatis et al. 2013b; Bienaymé et al. 2014). Here we confirm that the giant stars in RAVE can indeed be used as an unbiased sample. Piffl et al. (2014) fitted a full dynamical model of the Milky Way to the kinematics of the RAVE giants. They then tested if the resulting model would also correctly predict the kinematics of a sample of hot dwarf stars from RAVE and found a number of discrepancies. Their conclusion was that the thick disc distribution function in their model was too simplistic. However, Binney et al. (2014) also found that a similar dynamical model fitted to data from the GCS (Nordström et al. 2004) could reproduce the RAVE hot dwarf kinematics, but did not fit the RAVE giants. Since the GCS has a selection function that is different from that of the RAVE dwarfs, this implies that taking into account a more complicated volume correction for the hot dwarfs will not be enough to completely reconcile them with the model of Piffl et al. (2014). Hence a more complex distribution function for the thick disc, as argued for by the authors, seems still necessary.

We also illustrate that the quantified RAVE selection function can be used to generate mock-RAVE surveys from stellar population synthesis models, and in combination with code frameworks like GALAXIA, it can serve as a powerful tool to test Galaxy models against the RAVE data. The two versions of the RAVE selection function produced by this study (field-by-field and by HEALPIX pixel) will be made publicly available on the RAVE web site (https://www.rave-survey.org).

REFERENCES

Bailer-Jones C. A. L., et al., 2013, A&A, 559, A74
Bienaymé O., et al., 2014, A&A, 571, A92
Binney J., et al., 2014, MNRAS, 437, 351
Boeche C., et al., 2011, AJ, 142, 193
Bovy J., Rix H.-W., Liu C., Hogg D. W., Beers T. C., Lee Y. S., 2012, ApJ, 753, 148
Breddels M. A., et al., 2010, A&A, 511, A90
Burnett B., Binney J., 2010, MNRAS, 407, 339
Cutri R. M., et al., 2003, VizieR Online Data Catalog, 2246
DENIS Consortium 2005, VizieR Online Data Catalog, 2263
Epchtein N., et al., 1999, A&A, 349, 236
Gaia Collaboration et al., 2016, A&A, 595, A1
Gilmore G., et al., 2012, The Messenger, 147, 25
Górski K. M., Hivon E., Banday A. J., Wandelt B. D., Hansen F. K., Reinecke M., Bartelmann M., 2005, ApJ, 622, 759
Hambly N. C., et al., 2001, MNRAS, 326, 1279

Høg E., et al., 2000, A&A, 355, L27
Kordopatis G., 2015, IAU General Assembly, 22, 2252182
Kordopatis G., et al., 2011, A&A, 535, A107
Kordopatis G., et al., 2013a, AJ, 146, 134
Kordopatis G., et al., 2013b, MNRAS, 436, 3231
Kunder A., et al., 2017, AJ, 153, 75
Lewis I. J., et al., 2002, MNRAS, 333, 279
Majewski S. R., et al., 2015, preprint, (arXiv:1509.05420)
Matijevič G., et al., 2012, ApJS, 200, 14
Michalik D., Lindegren L., Hobbs D., 2015, A&A, 574, A115
Minchev I., et al., 2014, ApJ, 781, L20
Munari U., et al., 2014, AJ, 148, 81
Nidever D. L., et al., 2014, ApJ, 796, 38
Nordström B., et al., 2004, A&A, 418, 989
Piffl T., et al., 2014, A&A, 562, A91
Prusti T., 2012, Astronomische Nachrichten, 333, 453
Recio-Blanco A., et al., 2016, A&A, 585, A93
Robin A. C., Reylé C., Derrière S., Picaud S., 2003, A&A, 409, 523
Roeser S., Demleitner M., Schilbach E., 2010, AJ, 139, 2440
Schönrich R., Binney J., 2009, MNRAS, 399, 1145
Sharma S., Bland-Hawthorn J., Johnston K. V., Binney J., 2011, ApJ, 730, 3
Sharma S., et al., 2014, ApJ, 793, 51
Siebert A., et al., 2008, MNRAS, 391, 793
Siebert A., et al., 2011, AJ, 141, 187
Skrutskie M. F., et al., 2006, AJ, 131, 1163
Steinmetz M., et al., 2006, AJ, 132, 1645
Stonkutè E., et al., 2016, MNRAS, 460, 1131
Tonry J., Davis M., 1979, AJ, 84, 1511
Veltz L., et al., 2008, A&A, 480, 753
Williams M. E. K., et al., 2013, MNRAS, 436, 101
Wright E. L., et al., 2010, AJ, 140, 1868
Yanny B., et al., 2009, AJ, 137, 4377
Zacharias N., Finch C. T., Girard T. M., Henden A., Bartlett J. L., Monet D. G., Zacharias M. I., 2013, AJ, 145, 44
Zwitter T., et al., 2008, AJ, 136, 421
Zwitter T., et al., 2010, A&A, 522, A54

This paper has been typeset from a TEX/LATEX file prepared by the author.